Statistical and parametric studies on natural levees as weak points against leakages in river levees

Wenyue Zhang[a] and Akihiro Takahashi[a]*

[a] *Department of Civil and Environmental Engineering, Tokyo Institute of Technology, Tokyo, Japan*

Wenyue Zhang
Student, Department of Civil and Environmental Engineering,
Tokyo Institute of Technology,
ORCID: 0000-0003-2983-7376

Akihiro Takahashi*
Professor, Department of Civil and Environmental Engineering,
Tokyo Institute of Technology,
2-12-1-M1-3, Oh-okayama, Meguro, Tokyo, 152-8552, Japan
E-mail: takahashi.a.al@m.titech.ac.jp
ORCID: 0000-0003-1206-5066
* Corresponding author

Geotechnical and Geological Engineering, 40(11), 5643-5666, 2022

Original URL:

https://doi.org/10.1007/s10706-022-02238-y

Statistical and parametric studies on natural levees as weak points against leakages in river levees

Sandy natural levee deposits have been pointed out to provide seepage paths under river levees, which are largely related to the underseepage problems. However, few attempts have been taken to quantitatively study the relationship between the natural levees and the leakages in river levees. To capture the features of real natural levees, statistical studies are performed on the geometry and hydraulic conductivity of the micro-topographies along the Kinu River in Japan. By setting cases based on the retrieved data, a parametric study on the geometric and hydraulic parameters is performed by finite element seepage analysis. As a result, the embankment sitting on the landside of the natural levees is identified to be susceptible to leakages. In addition, rainfall and flooding are distinguished as the two driving forces of leakages depending on the hydraulic conductivity of the embankment bodies and the underneath foundations. The sandy natural levee deposits, with relatively high hydraulic conductivity, providing seepage paths for the under seepage, may magnify the effects of the seepage driven by the flooding, and lead to the classical backward erosion piping. Discussion and comments are addressed for the existing engineering practice in Japan.

Keywords: natural levees, micro-topographies, river levees, leakages, backward erosion piping

1. Introduction

During the 2019 Typhoon Hagibis, accompanied by which the highest daily precipitation was recorded in eastern and northern Japan, 142 cases of levee breaching occurred, causing around 64,000 hectares of submergences and 105 fatalities (FDMA, 2020; MLIT, 2020). According to the investigations, overflow, seepage flow, and scouring were recognized to be the major causes of the levee breaching (MLIT, 2019).

Backward erosion piping, usually referred to as “piping” or “leakage” in Japan, occurs when soil particles are detached by seepage flow at exit points, and finally leads to pipes reaching the riverside of the water retaining structures (USBR, 2019). Since the early studies by Terzaghi (1939), many studies have been performed by laboratory testing (Van Beek, 2015; Richard & Reddy, 2012; Fleshman & Rice, 2014; Negrinelli et al., 2016; Robbins et al., 2018), theoretical analyses (Sellmeijer, 1988; Rhee & Bezuijen, 1992), numerical simulation (Fujisawa et al., 2010; Wang et al., 2014; Vandenboer et al., 2014; Liang et al., 2017; Maeda et al., 2019), centrifugal modelling (Van Beek et al., 2010; Ito et al., 2021), and full-scale modelling (Sellmeijer et al., 2011; PWRI, 2014; Parekh et al., 2016). Based on the knowledge from the studies, guidelines on the management of levees have been set up (USACE, 2000; USACE, 2005; JICE, 2012).

Regretfully, with all the efforts paid, the existing evaluating methods of piping were found to be not able to correctly predict the piping failures in some cases (Kikumori, 2008). The main reason is that most of the studies were performed under idealized situations, with simplified structures and homogeneous soil. However, the real levees, constructed in different historical periods, and sitting on natural foundations, are far more complex than the idealized models. Especially, the foundations consisting of natural deposits of different micro-topographies are pointed out to play an important role in the triggering of piping (Kolb, 1975; Strange et al., 2016; Dunbar et al., 2018).

Natural levees, as one of the commonly seen micro-topographies in the alluvial environment in Japan, are the sandy or silty structures along the river channels deposited by the overbank flow during historical floods (Brierley & Fryirs, 2005). As shown in Fig. 1, it is a common practice to build river embankments on these elevated and well-drained berms (Itsukushima, 2018). However, it is repeatedly reported (Kuroki & Shinagawa, 2018), and statistically proven (PWRI, 2010) that the embankments sitting on natural levees are closely related to leakage events. Although the sandy natural levees have long been considered to provide seepage paths for the under seepage and were emphasized in the design guideline (JICE, 2012), few attempts have been made to quantitatively study the effects.

The scope of this study is to quantitatively evaluate the relationship between natural levees and piping from engineering points of view. The Kinu River in Japan, where a large number of leakage events during the storm in 2015 were believed to be related to natural levees (Kuroki & Shinagawa, 2018), is selected as an example for the study (Fig. 2). To capture the features of natural levees, statistical studies are performed on the geometry and hydraulic conductivity of the micro-topographies along the Kinu River. Based on the retrieved data, a series of parametric studies on the geometric and hydraulic parameters are performed by finite element seepage analysis. Finally, discussions are made based on the results from the numerical simulations and the existing practice in Japan.

2. Statistical studies on the geometry of the micro-topographies along the Kinu River

As shown in Fig. 3, the “levee” in this study consists of the artificially built “embankment” and the naturally formed elevated “berm” underneath. This study focuses on the elevations of the structures and the two-dimensional (2D) spatial relationship between the embankments and the underneath berms.

2.1: Source of data

An online Geographical Information System (GIS) is provided by the Geospatial Information Authority of Japan (GSI) (Fig. 4), in which a Digital Elevation Model (DEM) is included. In the studied area, the DEM has 5 m-mesh and an accuracy of 0.3 m in elevation.

In this statistical study, the data are retrieved by the following steps:

(1) Selecting the positions where elevation profiles are to be retrieved in the map.

The positioning in this study is based on the coordination system applied for rivers in Japan (MLIT, 2018), where the locations are usually presented in the form of “L/R 12.5k”, where “L” and “R” indicate left or right bank, the number is the distance measured from the estuaries, along the central line of the river, and “k” indicates kilometres.

In this study, data are retrieved from 0~53 km at the left and right banks along the Kinu River, with a spacing of around every 200~300 m.

(2) Retrieving the data by using the “sectional view” tool of the GIS.

This is performed from the downstream to the upstream, along the levees at the left and right banks respectively. In each focused position (data spot decided in Step 1), a path across the levee is manually selected by referring to the Elevation Map with a self-defined coloured scale and the aerial photos. Several trials may be made before the final judgement, ensuring that the selected path passes through the steepest slope at the riverside and the landside, which are supposed to be the critical paths for seepage. An elevation profile across the selected path will be automatically generated, in which the focused elements can be identified, including the toes of the embankment and the edges of the berm beneath. Elevations of particular points and the widths of the focused structure can be manually read and noted down from the elevation profile.

(3) Integrating the information for the locations where data are retrieved.

The categories of micro-topographies are noted based on the Landform Classification Map for Flood Control. Notes are taken if necessary, including whether there was any leakage event during the flood in 2015 (KRDB MLIT, 2016), the existence of artificial structures, or any other abnormalities.

In addition to the data retrieved directedly from the DEM, other data like the average elevation of the riverbed and the Highest Water Level (H.W.L.) are extracted from a report about the channel properties of the Kinu River (Research Institute of River Environment, 2009).

2.2: The "embankment & berm" model

A typical cross-section of the levees (L 23.1k) is shown in Fig. 5. The berms at the riverside are found to have stepped shapes, while the berms at the landside are found to have gentle slopes, which complies with the sedimentary mechanism of the overbank deposits and the erosional mechanism of the river.

According to the observations mentioned above, an idealized "embankment & berm" model is proposed, based on which the focused parameters are defined (Fig. 5). It is noticeable that the "berm" here may consist of the natural levee deposits or any other micro-topographies. In the model, the berm at the riverside is simplified to be a step, while the berm at the landside is simplified to be a slope.

The focused parameters in the proposed model are defined in Table 1.

2.3: Discussion on the retrieved data

By using the methodology introduced in Subsection 2.1, data are extracted from 145 spots at the left bank and 160 spots at the right bank. Among the 305 data spots, 216 of them (70.8%) are categorized as natural levees by the Landform Classification Map for Flood Control.

As shown in Fig. 6, the data retrieved from the DEM are not continuous. This is because in certain sections, mostly the sections where the river is directly restricted by the high terraces, no artificial embankments are found. Those sections are regarded to be out of the scope of this study.

Since the focus of this study is the relationship between natural levees and piping, the discussions and analysis on the spatial distribution of the natural levees and the characteristics of the river channel are not presented here. Instead, the retrieved data about the geometric characteristics of the embankments and the underneath berms will be used in Section 4 for a more realistic parametric study.

3. Statistical study on the hydraulic conductivity of the levees along the Kinu River

To have a better understanding of the hydraulic conductivity of the embankments and the natural levees, a statistical study on the levees along the Kinu River is performed.

3.1: Source of data

Based on the *Design Guideline for Levees* (MLIT, 2017), a series of investigations were performed on the levees along the governmentally regulated rivers in Japan, during which boreholes were bored and samples were collected. Mainly based on the newly performed investigations, also involving some old documents, a database about the soil of the levees was set up, from which (1) the borehole logs, (2) the summary of soil testing results, and (3) the soil profiles are referred to in this study.

The borehole logs are provided in the form of ordinary borehole log sheets, in which the soil classification at a certain depth can be read. In the focused segments (0~53 km) of the Kinu River, 164 borehole logs along the left bank and 180 borehole logs along the right bank are available.

The summary of soil testing results is provided in the form of spreadsheets, in which the basic soil properties of the samples collected at certain depths from the boreholes are provided. In the focused segments (0~53 km) of the Kinu River, 569 samples along the left bank and 571 samples along the right bank are available, while only among parts of them the hydraulic conductivities are estimated.

The soil profiles are provided in the form of estimated geological cross-sections as shown in Fig. 7. In the soil profiles, the soil with similar properties at a certain depth is regarded as a "layer", the naming of which indicates the formation (the capital letters, A = Alluvium, D = Diluvium, B/F = embankment/fill), the composition (the following letters, g = gravel, s = sand, c = clay, p = peat), and the sequence (the numbers) of the layer. In the focused segments (0~53 km) of the Kinu River, 33 soil profiles along the left bank and 33 soil profiles along the right bank are available, between which the spacing is around 1~2 km.

3.2: Processing of the data

As mentioned in Subsection 3.1, three kinds of materials are available from the database. In this statistical study, the mainly focused parameter, hydraulic conductivity is provided in the spreadsheets. However, the classification of the soil, the responding micro-topographies, and the relative positions of the layers are provided by other sources, without combining them together meaningful discussion cannot be made. Therefore, for every sample with hydraulic conductivity in the spreadsheets, the following processing is performed:

(1) Noting down the classification of the soil by referring to the borehole logs;

(2) Noting down the classification of micro-topographies in the responding spots by referring to the Landform Classification Map for Flood Control;

(3) Noting down the formation of corresponding layers (A/B/D) by referring to the soil profiles;

(4) Noting down whether the samples belong to the "seepage path" (explained below) by referring to the soil profiles.

Considering the conditions susceptible to leakages, the concept "seepage path" is raised here. As shown in Fig. 8, "seepage path" is defined as follows:

(1) Any continuous sandy/gravelly layers in the embankment;

(2) The continuous sandy/gravelly layers in the foundation close to the ground surface (with an impermeable blanket of less than 3 m).

After that, by referring to the borehole logs and the soil profiles, the parameters related to the seepage path are retrieved, including:

Thickness of the seepage paths T_S (m): Given that the layers are non-uniform, average values are taken among the thickness at the riverside, landside, and centre of the embankments. If there is no seepage path in the cross-section, $T_S = 0$.

Thickness of the impermeable layers above the seepage paths T_{NS} (m): The thickness at the centre of the embankment is taken. If there is no seepage path in the cross-section, $T_{NS} = H_l$.

Thickness of the covering impermeable blankets T_{cover} (m): Since the thin covering blankets are usually not recorded in the soil profiles in the database, only a few values are retrieved from the investigating report of the leakage spots observed in 2015 (KRDB MLIT, 2016).

3.3: Discussion on the retrieved data

In the newest guideline (JICE, 2012), in-situ tests are recommended for the foundations, and laboratory tests on the re-constituted samples are recommended for the embankment bodies. However, during the processing of the data, hydraulic conductivity in the database is found to be mainly estimated by the empirical Creager's method (728 out of 1,111 data). As a result, the discussions are mainly based on the data estimated by Creager's method, in which the estimating formulas for hydraulic conductivity k (m/s) based on the empirical data are given by Inazaki & Konishi (2010):

$$k = \begin{cases} 0.36D_{20}^{2.368} \times \frac{1}{100}, & if\ D_{20} > 0.03 \\ 0.0647D_{20}^{1.885} \times \frac{1}{100}, & if\ D_{20} < 0.03 \end{cases} \quad (1)$$

where D_{20} is the 20% passing grain size (mm).

With the retrieved data, to illustrate the relationship between the hydraulic features of natural levees and the leakage events, the spatial distribution of hydraulic conductivity in natural levees (NL) is presented with highlights on seepage paths and leakage events. The comments and findings on the retrieved data are as follows:

(1) The retrieved hydraulic conductivities scatter intensely along the river, from which obvious trends cannot be identified.

Since the data are retrieved all along the boreholes, it is not surprising that hydraulic conductivities in the same location vary in a large range. Given the difficulty to distinguish which layers belong to the natural levee deposits, as well as the inaccuracy of the estimating methods, it is regarded to be not feasible to directly relate hydraulic conductivity and the leakages.

(2) Leakage events in the foundations, especially severe boiling events, tend to occur in locations with continuous seepage paths through the foundation.

In Fig. 9 (a), most of the leakage events in the foundations are found to be related to the seepage paths through the foundation. Therefore, the existence of continuous permeable layers through the foundation is believed to be the critical condition of leakages rather than the hydraulic conductivity itself.

(3) Seepage paths through the embankments are also associated with leakage events.

It is found in Fig. 9 (b) that the leakage events through the embankments tend to occur in locations with continuous seepage paths. However, unlike the materials in the foundations, which are believed to be related to the corresponding micro-topographies, the materials in the embankments depend on the construction process, which is out of the scope of this study. Considering that the artificial embankments are built on elevated berms, another possibility is that some of the seepage paths in embankments consist of the natural materials in the foundations. It is common that the soil profiles based on the investigations after the leakages (KRDB MLIT, 2016) contradict the old documents, showing that parts of the embankment body previously regarded as artificial materials turn out to be natural materials (for example, L 20.15k and L21.5k in the Kinu River).

In summary, the data about the hydraulic characteristics of natural levees are retrieved, based on which the relationship between the seepage paths and the leakage events is revealed. Most importantly, the knowledge and the data achieved in the study will contribute to the parametric study in Section 4.

4. Parametric study on the natural levees underneath the embankments

In this section, a series of parametric studies are performed to quantitatively evaluate the relationship between natural levees and piping risk. The significance of parametric studies is that the simulations are performed based on the information achieved from the statistical studies, which ensures the representation of reality.

4.1: The simulated model

The "Kanto-Tohoku Heavy Rainfall" in 2015 (KRDB MLIT, 2016; Technical Committee on the Kinu River Levees, 2016), which led to a series of leakage events, is taken as the prototype of the simulations in the study. Based on the knowledge from the statistical studies and the prototype, the simulated model is built, as shown in Fig. 10.

In this model, the geometry of the embankment is set by referring to the cross-section at L 21.0k in the Kinu River (Technical Committee on the Kinu River Levees, 2016), at which breaching occurred in the 2015 Kanto-Tohoku Heavy Rainfall, and the suggested design values by the guideline (JICE, 2012).

The soil profile in the model is set based on the concept of the "seepage path". The model consists of (1) the silty embankment material Bc, (2) the sandy natural levee material As (the seepage path), (3) the clayey alluvial deposits Ac, and (4) the silty covering blanket on the surface of the embankment and the landside T. The hydraulic and mechanical parameters of the soil are set based on the field investigation at L 21.0k in the Kinu River (Technical Committee on the Kinu River Levees, 2016), as summarized in Table 2. To account for the anisotropy of hydraulic conductivity, following the common practice in Japan, $k_v/k_h = 1/3$ is applied to all the soil, where k_v is the vertical hydraulic conductivity (m/s), while k_h is the horizontal hydraulic conductivity (m/s) (Tanaka et al., 2017). To describe the unsaturated behaviour, the unsaturated soil property defined in the Japanese guideline (JICE, 2012; Fig. 11) is applied.

In the model, the focused geometric parameters (highlighted in Fig. 10) include: (1) the relative elevation of the embankment at the riverside H_r, (2) the relative elevation of the embankment at the landside H_l, (3) the thickness of the seepage path T_S, and (4) the height of the seepage path above the landside H_S. The last parameter H_S (m), defined as the elevation difference between the top of the seepage path and the embankment toe at the landside, can be calculated by $H_s = H_l - T_{NS}$. H_S is the parameter to describe the position of the seepage path.

Keeping the same with the practice in Japan, the simulations in the study consider both the effects of the precipitation and the river water level rising. The applied hydraulic loading in the simulations is set based on the "Kanto-Tohoku Heavy Rainfall" in 2015 (Technical Committee on the Kinu River Levees, 2016) and the Japanese guideline (JICE, 2012). As highlighted in Fig. 10, the varying head boundary is applied at the riverside; the constant head boundary is fixed at the landside; the bottom boundary is set impermeable, and the precipitation boundary is set for the unsubmerged surface. The temporal variation of the hydraulic loading is shown in Fig. 12. The hydraulic loading is divided into six stages as summarized in Table 3.

It is noticeable that: (1) the H.W.L. is taken as datum here so that the same hydraulic loading input can be applied for all the cases with variant geometry settings; (2) to ensure conservative situations and also to simplify the model, the river water level rises from and recovers to the elevation of the groundwater level (-7.00 m in Fig. 12), which is higher than the actual river water before and after the flooding (-10.00 m and -7.40 m in Fig. 12); (3) the groundwater level is taken as the level of the lowland behind the levee, which is determined from the statistical studies as introduced in Section 2.

4.2: Details about the simulations

In the parametric study, the finite element analysis is applied to numerically simulate the seepage process. The finite element analysis software PLAXIS 2D is controlled by the scripts written in Python so that the same template can be conveniently applied with different input geometric and hydraulic parameters (Bentley System, 2019). Transient flow analysis is performed in the plane strain model.

Given that the conditions with covering blankets are the more common cases in the Kinu River based on the investigations (KRDB MLIT, 2016), the index G/W is chosen as the index to describe the risk of piping, which is defined as:

$$G/W = (\rho_t g \cdot H)/(\rho_w g \cdot P) \quad (2)$$

Where, G = weight of the covering soil, W = uplifting pressure under the covering soil, g = acceleration of gravity (m/s^2), ρ_t = bulk density of the covering soil (kg/m^3), H = thickness of the covering soil (m), ρ_w = density of water = 1000 (kg/m^3), and P = pressure head under the covering soil (m).

As shown in Fig. 13, G/W is a kind of factor of safety against the uplifting seepage forces underneath the covering blanket. The smaller the value of G/W is, the larger the risk of piping is. A minimal G/W is screened out by Python script in time and space during a simulation. A minimal value of 1.0 is required for G/W by the Japanese guideline (JICE, 2012).

4.3: Effects of the geometry

In this subsection, studies on the geometry of the embankment and the underneath seepage path are presented. Given the difficulty to study the focused geometric parameters (Fig. 10) altogether, a series of studies are conducted on the parameters separately, following the philosophy of parsimony (starting from the simplicity and building up complexity gradually). Three groups of studies are performed, focusing on (1) the effects of the thickness of the seepage paths, (2) the effects of the position of the seepage paths, and (3) the effects of the elevation difference between the landside and the riverside. It should be noted that in all the simulated cases, the setting of parameters is based on the retrieved data from the statistical studies, which are illustrated in detail in Appendix A.

4.3.1: Effects of the thickness of the seepage path

Firstly, the focus is cast on the effects of the thickness of the seepage paths. As highlighted in Fig. 14, the simulated cases have different thicknesses of the seepage path T_S (Table 4), while all the other geometric parameters are kept constant. The hydraulic parameters of the soil follow the ones summarized in Table 2.

The results of the simulations are shown in Fig. 15. The x-axis in the figure is the thickness of the seepage path T_S normalized by the relative elevation of the embankment at the landside H_l. It is found that G/W drops with the increasing thickness of the seepage path, indicating a larger piping risk for a thicker seepage path.

4.3.2: Effects of the position of the seepage path

For the embankments built on the elevated berms, it is possible that the parts that appeared to be the embankment bodies in geometry consist of the natural levee deposits. Therefore, the seepage paths may not be only located in the foundation but may also pass through the embankment bodies.

The study is performed on the effects of the position of the seepage path. As shown in Table 5, two groups of cases with a thickness of the seepage path T_S of 3 m and 4 m are set. In all the cases of this study, the relative elevations of the embankment at the landside and the riverside H_l and H_r are kept constant, while the positions of the seepage path are determined by the height of the seepage path above the landside H_S (Fig. 16). In all the cases, the hydraulic parameters of the soil follow the ones summarized in Table 2.

The simulated results are presented in Fig. 17. The x-axis in the figures is the heights of the seepage path above the ground H_S normalized by the thickness of the seepage path T_S. It is found that, although the G/W values fluctuate with H_S, the variation is not considered to be large enough, especially compared with the difference caused by the thickness of the seepage path. Therefore, the position of the seepage path is not regarded as the determinant factor for the piping risk.

4.3.3: Effects of the elevation difference between the landside and the riverside

In the statistical study by Kuroki & Shinagawa (2018), it was concluded that leakages tend to occur at locations with riverbanks higher than the protected side behind the levees. In the model, this is corresponding to the larger relative elevation of the embankment at the landside than the elevation difference at the riverside ($H_l > H_r$, or $\Delta H = H_r - H_l < 0$).

The study is performed on the elevation difference between the landside and the riverside. As shown in Table 6, two groups of cases with a relative elevation of the embankment at the landside H_l of 4 m and 5 m are included. The relative elevation of the toe of the embankment at the landside to that at the riverside ΔH is calculated for each case ($\Delta H = H_r - H_l$). As illustrated in Fig. 18, the other parameters are kept constant in all the cases of this study (T_S = 3 m, H_S = 1 m), while the varying parameters are highlighted. In all the cases, the hydraulic parameters of the soil follow the ones summarized in Table 2.

The simulated results are presented in Fig. 19. The x-axis in the figures is the relative elevation of the toe of the embankment at the landside to that at the riverside ΔH normalized by the relative elevation of the embankment at the landside H_l. It is found that:

(1) The piping risk rises drastically as the relative elevation of the embankment at the landside H_l increases. Considering that larger H_l means larger head difference, which is directly related to the piping risk, the finding is regarded to consist with the expectation.

(2) The piping risk drops as the relative elevation of the toe of the embankment at the landside to that at the riverside ΔH increases. In another word, the piping risk is larger for the cases with higher foundations at the riverside. However, the effects of ΔH are not so significant compared to the effects of the relative elevation of the embankment at the landside H_l, especially for the cases with relatively large H_l values ($H_l = 5$ m).

4.3.4: Summary

In the study on the effects of the geometry of the "embankment & berm" model, it is found that:

(1) Among the focused geometric parameters, the relative elevation of the embankment at the landside H_l and the thickness of the seepage path T_S are the determinant factors of the piping risk. The piping risk increase with the increasing H_l and T_S. The levee typically susceptible to leakages is illustrated in Fig. 20, where the embankment is built on the landside of a berm consisting of sandy natural levee deposits, leading to relatively large H_l and T_S. This model is similar to the cross-sections where leakage events with severe boiling were observed along the Kinu River (KRDB MLIT, 2016).

(2) Other geometric parameters like the height of the seepage path above the ground H_S and the relative elevation of the toe of the embankment at the landside to that at the riverside ΔH are found not to have determinant effects on the piping risk G/W.

4.4: Effects of the hydraulic conductivity

4.4.1: Numerical simulations

In this subsection, the study is performed on the effects of the seepage paths. All the geometric parameters are kept the same with Case 2-2 (T_S = 3 m, H_S = 1 m, H_l = H_r = 5 m, ΔH = 0 m, as shown in Fig. 21), while different hydraulic conductivities are applied in different cases, as summarized in Table 7. The relative hydraulic conductivity R_k is defined as the ratio of the vertical hydraulic conductivity in the seepage path (the As layer) to the vertical hydraulic conductivity in the embankment body (the Bc layer):

$$R_k = (k_v \text{ [As]})/(k_v \text{ [Bc]}) \quad (3)$$

In Table 7, three groups of cases are set: (1) the cases with R_k = 1, (2) the cases with R_k = 20, and (3) the cases with R_k = 100. In each group, cases with different vertical hydraulic conductivity in the embankment body k_v [Bc] are included to consider the large variation in the estimated hydraulic conductivity. It is noted that the hydraulic conductivity of the T layer and the Ac layer, as well as the unsaturated characteristics of all the soil, still follow the settings in Table 2.

To distinguish the effects of the flooding and the rainfall, besides the simulations following the process illustrated in Subsections 4.1 & 4.2, another set of simulations are performed on all the cases, keeping all the other settings the same, but with only the rainfall as the hydraulic loading. In these simulations, the water level is kept as the initial value along the time, while the rainfall in Fig. 12 is applied. Finally, the results (index for piping risk G/W) from the two sets of simulations (with flooding + rainfall, and with rainfall only) are compared. The small difference between the G/W values from the two sets of simulations indicates that the flooding does not contribute much to the piping risk, while the large difference indicates that the flooding is the main driving force of the piping risk.

In Fig. 22, the index for piping risk G/W is plotted against the vertical hydraulic conductivity in the embankment bodies k_v[Bc]. The results from the simulations with rainfall and flooding (Rain + Flood) are plotted in solid lines, while the results from the simulations with only the rainfall as hydraulic loading (Rain only) are plotted in dashed lines. It is found that:

(1) The distinction between the effects of flooding and rainfall can be made.

In the figure, the contribution of the flooding to the piping risk can be distinguished from the difference between the solid lines and the dashed lines. Looking at the lines with the same colour (the cases with the same relative hydraulic conductivity R_k), it is found that when the hydraulic conductivity is lower than a certain level (around 1.0E-5 m/s for R_k = 1, around 1.0E-6 m/s for R_k = 20, and around 2.0E-7 m/s for R_k = 100), the solid line and the dashed line converge together, while with higher hydraulic conductivity, the solid line gradually separates from the dotted line and gives lower G/W values (larger piping risk).

(2) Depending on the relative hydraulic conductivity R_k, the seepage paths magnify the effects of the flooding.

Comparing the lines with different colours, it is found that the separating spots of the solid lines and the dashed lines differ among the groups with different R_k values. In the group with R_k = 1 (in other words, no seepage path), a k_v[Bc] value of around 1.0E-05 m/s is needed for the seepage from the riverside to contribute to the piping risk, while in the group with R_k = 100 (the cases with highly seepage paths), the seepage from the riverside starts to contribute to the piping risk with k_v[Bc] value of around 2.0E-07 m/s.

To look into the mechanism behind this, the distributions of flow velocity in different cases (with flooding + rainfall) are compared in Fig. 23. This figure reveals the followings:

(1) The contribution of the flooding and the rainfall to the uplifting forces at the landside can be distinguished.

In the cases with very low transmissivity (the measure of the ability of water to transmit horizontally), like Case 4-7 and Case 4-11, the seepage from the riverside cannot penetrate the levees (embankment bodies and the foundations) and hence does not contribute to the piping risk. The accumulation of pore water pressure is mainly caused by the surface infiltration from the rainfall at the landside. In the cases with relatively large transmissivity (Case 4-10, Case 4-14), the flow patterns in the soil are dominated by the seepage from the riverside.

(2) The seepage paths magnify the effects of the seepage from the riverside.

Comparing the cases with the same k_v[Bc] but different R_k (for example, Case 2-2 and Case 4-11), it is found that the seepage paths allow the underground seepage to go further towards the landside, and hence magnify the effects of the seepage from the riverside.

4.4.2: Discussion and comments

A quantitative study on the effect of hydraulic conductivity reveals the followings:

(1) Depending on the hydraulic conductivity of the embankments and the foundations, the leakages at the landside may be driven by: (a) the seepage from the riverside due to the flooding, (b) the surface infiltration due to the rainfall, or (c) the combined effect of the flooding and the rainfall (Fig. 24).

(2) The failure mechanisms are believed to be different when the driven forces are different. When the leakage is mainly driven by the seepage due to the flooding, the classical backward erosion piping may develop. In contrast, when the leakage is mainly driven by the surface infiltration due to the rainfall, the classical backward erosion piping is unlikely to develop. According to the field observations in the Kinu River (KRDB MLIT, 2016), cracks, local collapse, or slope failures are the possible consequences of the leakages driven by the rainfall. Apart from the commonly recognized sliding failure, another kind of failure called “local failure” (Akai, 1956; Wu et al., 2017; Midgley et al., 2013) or “progressive failure” (PWRI, 2015) was identified. According to some middle-scale and

small-scaled modelling experiments, this kind of failure occurred at the shallow part of the embankment slope and gradually progressed upward (PWRI, 2015). Up to now, there is no well-recognized estimating theory or practical regulation about “progressive failure”.

(3) The natural levees, which are believed to provide seepage paths for under seepage, may magnify the effects of the seepage driven by the flooding. Therefore, the embankments sitting on the natural levees are believed to be more susceptible to backward erosion piping.

As discussed above, the failure mechanisms may differ in the cases dominated by different driving forces. However, the evaluating methods against piping in Japan (JICE, 2012) focused on the initiation rather than the progression of piping. Therefore, the existing engineering practice is considered to be not capable of correctly capturing the “risk”, which determines the urgency of sequential countermeasures.

Besides the evaluating methods, appropriate countermeasures may differ for the cases dominated by different driving forces. For example, according to in-situ monitoring and large-scaled experiments (Nakata et al., 2008; Takeshita & Torigoe, 2020), the “blocking” methods like the sheet piles may be suitable against seepage from the riverside due to flooding, while the “dissipating” methods like the drainage toes may be suitable against surface infiltration due to the rainfall.

Given the disadvantages mentioned above, the followings are suggested:

(1) For the evaluating methods against piping, not only should the absolute values of the focused indexes be checked, but the driving forces of the leakages should also be distinguished. For the cases mainly driven by flooding, the classical theories about piping can be applied, while for the cases mainly driven by rainfall, a new understanding is needed.

(2) More accurate estimations of the hydraulic conductivity are needed so that more appropriate countermeasures can be decided based on the correct understanding of the seepage behaviour.

5. Conclusions

In this study, an attempt was made to quantitatively study the naturally formed structures. During the study, efforts are paid to adhere to reality as much as possible. Firstly, statistical studies along the Kinu River provide a basic understanding of the characteristics of natural levees. The retrieved data from the statistical studies ensure the reasonability of the simulated model and the case settings. Discussions and comments are made by associating with the engineering practice in reality. The main conclusions include:

(1) The assumed “embankment & berm” model is confirmed by the realistic data. The elevated berms consisting of the naturally formed alluvial deposits are identified as important parts of the levees.

(2) In the statistical study on hydraulic conductivity, the seepage paths through the embankment bodies or in the foundations are found to be closely associated with the leakage events.

(3) Among the focused geometric parameters, the relative elevation of the embankment at the landside and the thickness of the seepage path are the determinant factors of the piping risk. The embankments built on the landside of a berm consisting of sandy natural levee deposits are believed to be susceptible to leakages.

(4) Flooding and rainfall are distinguished to be the two driving forces of leakages, under the effects of which different failure mechanisms are considered to occur.

(5) The natural levees, providing the seepage paths for under seepage, may magnify the effects of the seepage driven by the flooding. Therefore, the embankments sitting on the natural levees are believed to be more susceptible to the backward erosion piping. More attention should be paid to the management of river levees in the future.

(6) This study is an attempt to combine realistic statistics and numerical analysis. A similar methodology can be applied to study other micro-topographies related to the leakages, like the abandoned river channels, back swamps, and sand dunes.

Appendix A

In Subsection 4.3, it is mentioned that to ensure that the simulated model correctly reflects the characteristics of natural levees, the data retrieved in the statistical studies are referred to when setting the cases in the parametric studies. In this appendix, distributions of the retrieved geometric and hydraulic parameters in the representative section (7~30 km along the left bank of the Kinu River) are presented. The representative section is selected because those natural levees are widely distributed, while cases of seepages through the seepage paths were observed in this section.

The distributions of the geometric and hydraulic parameters in the representative sections are shown in Fig. 25~31. In the figures, several concepts are defined to capture the characteristics of the distributions: the "range" here is the range within which all the data are distributed; the "typical values" here is the range where the data concentrate; and the "peak" here is the peak of the distribution. These features are visually distinguished from the distributions and summarized in Table 8 (Definitions of the parameters are illustrated in Fig. 5 and Fig. 8). It is seen that some of the values are blanked due to the inapplicability of the concepts to the scattered distributions, or the lack of information. Although the method seems to be tedious, it is believed to be more reasonable than trying to describe the distributions by applying a single mathematical model.

Besides the data from the statistics studies, data from the spots with severe sand boils are also summarized in Table 8. Retrieved from the soil profiles in the investigating reports (KRDB MLIT, 2016), these data are more accurate, with more details, and are believed to reflect the critical conditions of the failure spots. In the following parametric study, these data are taken as important references.

Reference

Akai, K (1956) About the local failure at the landside of the embankment caused by the seepage flow (In Japanese). Proceedings of JSCE 36: 44-49. https://www.jstage.jst.go.jp/article/jscej1949/1956/36/1956_36_44/_pdf. Accessed 10 January 2022

Bentley System (2019) Manuals archive – PLAXIS. Bentley Communities. https://communities.bentley.com/products/geotech-analysis/w/plaxis-soilvision-wiki/50826/manuals-archive---plaxis. Accessed 10 January 2022

Bonelli S (Ed.) (2013) Erosion in geomechanics applied to dams and levees. John Wiley & Sons

Brierley GJ, Fryirs KA (2005) Geomorphology and river management: applications of the river styles framework. John Wiley & Sons

Dunbar JB, Ensign AL, Torres N, Corcoran MK (2018) Analysis and Comparison of Documented Seepage and Sand Boil Events on the Lower Mississippi River from 1937 to 2011. Volume 1, Main text. USACE. http://hdl.handle.net/11681/28597

Fire and Disaster Management Agency (FDMA) (2020) Damage caused by the Eastern Japan Typhoon in 2019 and the heavy rain due to the front, as well as the response of the emergent agency (the 67th report) (in Japanese). https://www.fdma.go.jp/disaster/info/items/taihuu19gou67.pdf. Accessed 10 January 2022

Fleshman MS, Rice JD (2014) Laboratory modeling of the mechanisms of piping erosion initiation. Journal of geotechnical and geoenvironmental engineering 140(6): 04014017.

Fujisawa K, Murakami A, Nishimura SI (2010) Numerical analysis of the erosion and the transport of fine particles within soils leading to the piping phenomenon. Soils and foundations, 50(4): 471-482.

Inazaki T, Konishi C (2010) Relationship between permeability and grain size characteristics of substrata of levee systems (in Japanese). Advances in River Engineering, 16: 377-382. http://library.jsce.or.jp/jsce/open/00906/2010/16-0377.pdf. Accessed 10 January 2022

Ito Y, Noda S, Takahashi A, Horikoshi K (2021) Measurement techniques for capturing piping-induced deformation of levees in centrifuge model. In: Proceedings of the 10th International Conference on Scour and Erosion, Washington D.C., USA, pp 923-930

Itsukushima R (2018) Countermeasures against floods that exceed design levels based on topographical and historical analyses of the September 2015 Kinu River flooding. Journal of Hydrology: Regional Studies 19: 211-223.

Japan Institute of Country-ology and Engineering (JICE) (2012) Guideline for the structural evaluation of levees (in Japanese). http://www.jice.or.jp/cms/kokudo/pdf/tech/material/teibou_kouzou02.pdf. Accessed 10 January 2022

Kanto Regional Development Bureau, Ministry of Land, Infrastructure, Transport and Tourism (KRDB MLIT) (2016) Materials for the 4th Technical Committee on the Kinu River Dike: Report for the detail investigation of the leakage spots in the levees (in Japanese). https://www.ktr.mlit.go.jp/ktr_content/content/000642509.pdf. Accessed 10 January 2022

Kikumori Y (2008) Study on Accuracy Improvement of Safety Evaluation of Seepage Failure of River Levees (In Japanese). Technical note of National Institute for Land and Infrastructure Management No 441. http://www.nilim.go.jp/lab/bcg/siryou/tnn/tnn0441pdf/ks0441.pdf. Accessed 10 January 2022

Kolb CR (1975) Geologic control of sand boils along Mississippi River levees. ARMY ENGINEER WATERWAYS EXPERIMENT STATION VICKSBURG MS. https://apps.dtic.mil/sti/pdfs/ADA014274.pdf. Accessed 10 January 2022

Kuroki T, Shinagawa S (2018) Damages caused by Kanto-Tohoku heavy rainfall in September 2015 and Micro-landform of the Kinu River (In Japanese). Bulletin of University of Teacher Education Fukuoka. Part II, Social sciences (67): 1-11. https://fukuoka-edu.repo.nii.ac.jp/?action=pages_view_main&active_action=repository_view_main_item_detail&item_id=849&item_no=1&page_id=13&block_id=21. Accessed 10 January 2022

Liang Y, Yeh TCJ, Wang YL, Liu M, Wang J, Hao Y (2017) Numerical simulation of backward erosion piping in heterogeneous fields. Water Resources Research 53(4): 3246-3261.

Maeda K, Nishimura M& Takatsuji M (2018) Micro-macro modelling of piping and internal erosion in river levee. In Scour and Erosion IX: Proceedings of the 9th International Conference on Scour and Erosion (ICSE 2018), November 5-8, 2018, Taipei, Taiwan, pp 353). CRC Press

Midgley TL, Fox GA, Wilson GV, Heeren DM, Langendoen EJ, Simon A (2013) Seepage-induced streambank erosion and instability: in situ constant-head experiments. Journal of Hydrologic Engineering 18(10): 1200-1210. https://ascelibrary.org/doi/abs/10.1061/(ASCE)HE.1943-5584.0000685

Ministry of Land, Infrastructure, Transport and Tourism (MLIT) (2017) Design Guideline for Levees (in Japanese). https://www.mlit.go.jp/river/shishin_guideline/bousai/gijyutukaihatu/pdf/teibou_sekkei.pdf. Accessed 10 January 2022

MLIT (2018) The coordination system for rivers (in Japanese). https://www.ktr.mlit.go.jp/ktr_content/content/000680105.pdf. Accessed 10 January 2022

MLIT (2019) The damages caused by Typhoon No. 19 in 2019. https://www.mlit.go.jp/river/shinngikai_blog/shaseishin/kasenbunkakai/shouiinkai/kikouhendou_suigai/1/pdf/11_R1T19niyoruhigai.pdf. Accessed 10 January 2022

MLIT (2020) The lost caused by flooding disasters in 2019 reached the peak in the historical statistics accompanied with the typhoon in eastern Japan in 2019: The press release for the lost in 2019 (provisional values) (in Japanese). https://www.mlit.go.jp/report/press/content/001359046.pdf. Accessed 10 January 2022

Nakata T, Kawai M, Sato K (2008) A study on the seepage experiments using an actual levee (in Japanese). Oyo Technical Report (28): 31-41. https://www.oyo.co.jp/oyocms_hq/wp-content/uploads/2014/12/2008_03.pdf. Accessed 10 January 2022

Negrinelli G, Van Beek VM, Ranzi R (2016) Experimental and numerical investigation of backward erosion piping in heterogeneous sands. In Scour and Erosion: Proceedings of the 8th International Conference on Scour and Erosion (Oxford, UK, 12-15 September 2016) 473. CRC Press.

Parekh, M. L, Kanning, W, Bocovich, C, Mooney, M. A, & Koelewijn, A. R (2016) Backward erosion monitored by spatial–temporal pore pressure changes during field experiments. Journal of Geotechnical and Geoenvironmental Engineering 142(10): 04016050.

Public Works Research Institute (PWRI) (2010) Research on the investigation methods on the hydraulic characteristics of the foundation of levees (in Japanese). https://www.pwri.go.jp/jpn/results/report/report-project/2010/pdf/pro-2-3.pdf. Accessed 10 January 2022

PWRI (2014) Research on the countermeasures against hiving in levees by large-scale modelling (in Japanese). https://www.pwri.go.jp/team/smd/pdf/report4267.pdf. Accessed 10 January 2022

PWRI (2015) Experiments on the progressive failures from the toes of the river embankment caused by the seepage flow (In Japanese). https://www.pwri.go.jp/team/smd/pdf/report4300.pdf. Accessed 10 January 2022

Research Institute of River Environment (2009) Study on the channel properties and channel regulation of the Kinu River: The river with exposed diluvium (in Japanese). The River Foundation. https://www.kasen.or.jp/Portals/0/pdf_kasen03/study02b_25.pdf. Accessed 10 January 2022

Rhee CV, Bezuijen A (1992) Influence of seepage on stability of sandy slope. Journal of geotechnical engineering 118(8): 1236-1240.

Richards KS, Reddy KR (2012) Experimental investigation of initiation of backward erosion piping in soils. Géotechnique 62(10): 933-942.

Robbins BA, van Beek VM, López-Soto JF, Montalvo-Bartolomei AM., Murphy J (2018) A novel laboratory test for backward erosion piping. International Journal of Physical Modelling in Geotechnics 18(5): 266-279.

Sellmeijer JB (1988) On the mechanism of piping under impervious structures (PhD thesis).

https://edepot.wur.nl/366746. Accessed 10 January 2022

Sellmeijer H, de la Cruz JL, van Beek VM, Knoeff H (2011) Fine-tuning of the backward erosion piping model through small-scale, medium-scale and IJkdijk experiments. European Journal of Environmental and Civil Engineering 15(8): 1139-1154.

Strange RC, Corcoran MK, Dunbar JB, Schmitz D (2016) The Influences of Geologic Depositional Environments on Sand Boil Development, Tara Wildlife Lodge Area in Mississippi. US Army Engineer Research and Development Center Vicksburg United States. https://apps.dtic.mil/sti/pdfs/AD1006973.pdf. Accessed 10 January 2022

Takeshita Y, Torigoe Y (2020) Quasi-real-time prediction of seepage flow behavior in river levee during flood by artificial neural network using deep learning (in Japanese). Proceedings of JSCE C (Geotechnical engineering), 76(4), 340-349.

Tanaka T, Nonomura K, Togashi R, Uno C (2017) Effects of anisotropic permeability of soil on characteristics of seepage flow and stabilities against seepage failure and slide of dam slope (in Japanese). Report of Research Center for Urban Safety and Security Kobe University 21: 289-298. http://www.lib.kobe-u.ac.jp/repository/81011558.pdf. Accessed 10 January 2022

Technical Committee on the Kinu River Levees (2016) Report of the Technical Committee on the Kinu River Dike (in Japanese). MLIT. https://www.ktr.mlit.go.jp/ktr_content/content/000643703.pdf. Accessed 10 January 2022

Terzaghi K (1939) Soil mechanics–A new chapter in Engineering Science. The 45th James Forrest Lecture. Journal of the Institution of Civil Engineers *12*: 106-142

US Army Corps of Engineers (USACE). (2000) Design and Construction of Levees. https://www.publications.usace.army.mil/Portals/76/Publications/EngineerManuals/EM_1110-2-1913.pdf. Accessed 10 January 2022

USACE (2005) Engineering and design: Design guidance for levee underseepage. https://www.mvn.usace.army.mil/Portals/56/docs/engineering/HurrGuide/ETL_1110-2-569_%20DESIGN_GUIDANCE_FOR_LEVEE_UNDERSEEPAGE_May_2005.pdf. Accessed 10 January 2022

US Bureau of Reclamation (USBR) (2019) Internal Erosion Risks for Embankments and Foundations. https://www.usbr.gov/ssle/damsafety/risk/BestPractices/Chapters/D6-InternalErosionRisksForEmbankmentsAndFoundationsWithAppendices.pdf. Accessed 10 January 2022

Van Beek VM, Bezuijen A, Zwanenburg C (2010) Piping: Centrifuge experiments on scaling effects and levee stability. Physical Modelling in Geotechnics. ISBN 978-0-415-59288, 8: 183-187

Van Beek, V. M. (2015). Backward erosion piping: initiation and progression (PhD thesis). https://repository.tudelft.nl/islandora/object/uuid:4b3ff166-b487-4f55-a710-2a2e00307311. Accessed 10 January 2022

Vandenboer K, van Beek V, Bezuijen A (2014) 3D finite element method (FEM) simulation of groundwater flow during backward erosion piping. Frontiers of Structural and Civil Engineering 8(2): 160-166.

Wang DY, Fu XD, Jie YX, Dong WJ, Hu D (2014) Simulation of pipe progression in a levee foundation with coupled seepage and pipe flow domains. *Soils and Foundations*, *54*(5), 974-984.

Wu LZ, Zhou Y, Sun P, Shi JS, Liu GG, Bai LY (2017) Laboratory characterization of rainfall-induced loess slope failure. *Catena*, *150*, 1-8.

Statement & Declarations

Funding

Author Wenyue Zhang has received support from Monbukagakusho (Ministry of Education, Culture, Sport, Science and Technology) Scholarship for international graduate students.

Competing interests

The authors have no relevant financial or non-financial interests to disclose.

Author Contributions

Both authors contributed to the study conception and design. Data collection and numerical analysis were performed by Wenyue Zhang. The first draft of the manuscript was written by Wenyue Zhang and both authors reviewed and edited the manuscript. Both authors read and approved the final manuscript.

Data availability

The data that support the findings of this study are openly available in:

Geospatial Information Authority of Japan (GSI) at

https://www.gsi.go.jp/top.html

National Institute for Land and Infrastructure Management (NILIM) at

http://www.nilim.go.jp/lab/fbg/download/geo_download/geo_download.html

Tables

Table 1 Definition of the geometric parameters of the "embankment & berm" model.

Parameter	Name	Definition
H_r (m)	Relative elevation of the embankment at the riverside	H_r is defined as the elevation difference between the top of the embankment (Point 3 in Fig. 7) and the toe of the embankment (Point 2) at the riverside.
H_l (m)	Relative elevation of the embankment at the landside	Similar to H_r, H_l is defined as the elevation difference between Points 3 & 4 at the landside.
ΔH (m)	Relative elevation of the toe of the embankment at the landside to that at the riverside	ΔH is defined as the elevation difference between the toe of the embankment at the landside and the riverside (Points 4 & 2), which can also be calculated by $\Delta H = H_r - H_l$. ΔH>0 indicates that the toe of the embankment at the landside is higher than that at the riverside.
T_r (m)	Berm thickness at the riverside	The thickness is defined as the elevation difference between the toe of the embankment (Point 2) and the toe of the berm (Point 1).
T_l (m)	Berm thickness at the landside	Similar to T_r, T_l is defined as the elevation difference between Points 4 & 5 at the landside.
W_r (m)	Berm width at the riverside	The width is defined as the distance between the toe of the embankment and the toe of the berm at the riverside (Points 2 & 1). In the case where there is no berm underneath the embankment, or the embankment locates at the edge of the berm at the riverside, $W_r = 0$.
W_l (m)	Berm width at the landside	Similar to W_r, W_l is defined as the distance between Points 4 & 5 at the landside.
W_e (m)	Embankment width	The width of the embankment is defined as the distance between the toe of the embankment at the riverside and the landside (Points 2 & 4).
α_r (°)	Slope of the berm at the riverside	The parameter is defined to describe the steepness of the berm at the riverside. $\alpha_r = \arctan(T_r/W_r)$. In the case where there is no berm underneath the embankment, or the embankment locates at the edge of the berm at the riverside ($W_r = 0$), $\alpha_r = 0$.
α_l (°)	Slope of the berm at the landside	Similar to α_r, $\alpha_l = \arctan(T_l/W_l)$. $\alpha_l = 0$ when $W_l = 0$.

Table 2 Hydraulic parameters of the soil in the simulated model.

Soil layer	Saturated unit weight γ_{sat} $(\mathrm{kN/m^3})$	Vertical hydraulic conductivity k_v $(\mathrm{m/s})$	Unsaturated characteristics
Bc	18	2.0E-06	[M], [C]
As	17	4.0E-05	[SF]
Ac	18	1.0E-07	[M], [C]
T (Cover)	18	2.0E-06	[M], [C]

Table 3 Six stages of the hydraulic loading.

Stage	Hydraulic loading	Duration
I	Long-term rainfall	0~187 hr
II	Intense rainfall	187~210 hr
III	Intense rainfall + Water level rising	210~224 hr
IV	Intense rainfall + H.W.L.	224~228 hr
V	Water level dropping	228~245 hr
VI	After the flood	245~250 hr

Table 4 Case settings in the study on the effects of the thickness of the seepage path.

Cases	T_S (m)
1-1	1
1-2	2
1-3	3
1-4	4
1-5	5
1-6	8
1-7	10

Table 5 Case settings in the study on the effects of the position of the seepage path.

Cases	T_S (m)	H_S (m)
1-3	3	0
2-1	3	0.5
2-2	3	1
2-3	3	1.5
2-4	3	2
1-4	4	0
2-5	4	0.5
2-6	4	1
2-7	4	1.5
2-8	4	2
2-9	4	3

Table 6 Case settings in the study on the effects of the elevation difference between the landside and the riverside.

Cases	H_r (m)	H_l (m)	ΔH (m)
3-1	3	4	-1
3-2	4	4	0
3-3	5	4	1
3-4	6	4	2
3-5	7	4	3
2-2	5	5	0
3-6	6	5	1
3-7	7	5	2

Table 7 Case settings in the study on the effects of the seepage paths.

Case	R_k	k_v[Bc] (m/s)
4-1	1	2.0E-07
4-2	1	1.0E-06
4-3	1	2.0E-06
4-4	1	1.0E-05
4-5	1	3.0E-05
4-6	1	1.0E-04
4-7	20	2.0E-07
4-8	20	1.0E-06
4-9	20	1.4E-06
2-2	20	2.0E-06
4-10	20	1.0E-05
4-11	100	2.0E-07
4-12	100	4.5E-07
4-13	100	1.0E-06
4-14	100	2.0E-06

Table 8 Features of data distributions in the representative section and the values in the spots with severe sand boils.

Parameters	From the statistical studies					From the spots with severe sand boils (Technical Committee on the Kinu River Dike, 2016; KRDB MLIT, 2016)			
	Range		Typical values		Peak	Coordination (km)			
	Min	Max	Min	Max		L 13.07-13.2k	L 20.15k	L 20.27k	L 21.5k
H_r (m)	2.5	9.0	3.0	7.0	5.0	4.3	6.8	5.2	5.5
H_l (m)	2.0	7.0	3.2	5.5	4.2	3.4	4.8	3.8	4.4
ΔH (m)	-1.8	4.0	-0.75	1.0	0.0	0.9	2.0	1.5	1.1
α_r (°)	0.0	16.2	0.0	5.5	0.1	17	4.8	6.8	5.4
α_l (°)	0.0	4.0	0.10	0.60	0.30	0.17	0.10	0.16	0.11
T_r (m)	0.0	5.2	2.0	4.0	2.4	3.0	0.9	2.4	1.9
T_l (m)	0	4.5	1.8	3.8	2.6	3.6	2.0	2.6	2.8
W_r (m)	5	325	5	55	12	10	5.0	20	20
W_l (m)	0	1425	200	475	362	700	1170	900	1400
T_S (m)	0	11.5	--	--	--	2.7	2.8	2.3	2.2
T_{NS} (m)	0	9.4	--	--	4.5	2.7	3.7	2.4	4.0
T_{cover} (m)	--	--	--	--	--	0.25	0.20	0.20	0.70

Figures

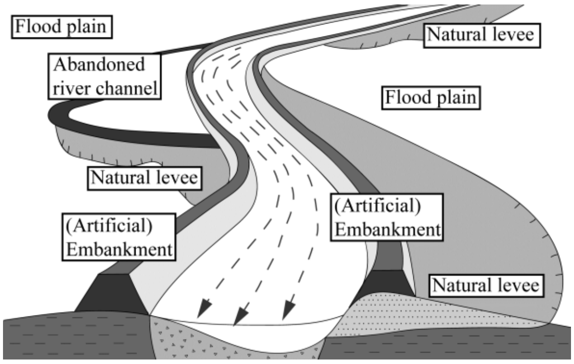

Figure 1. Schematic illustration of natural levees in the floodplain.

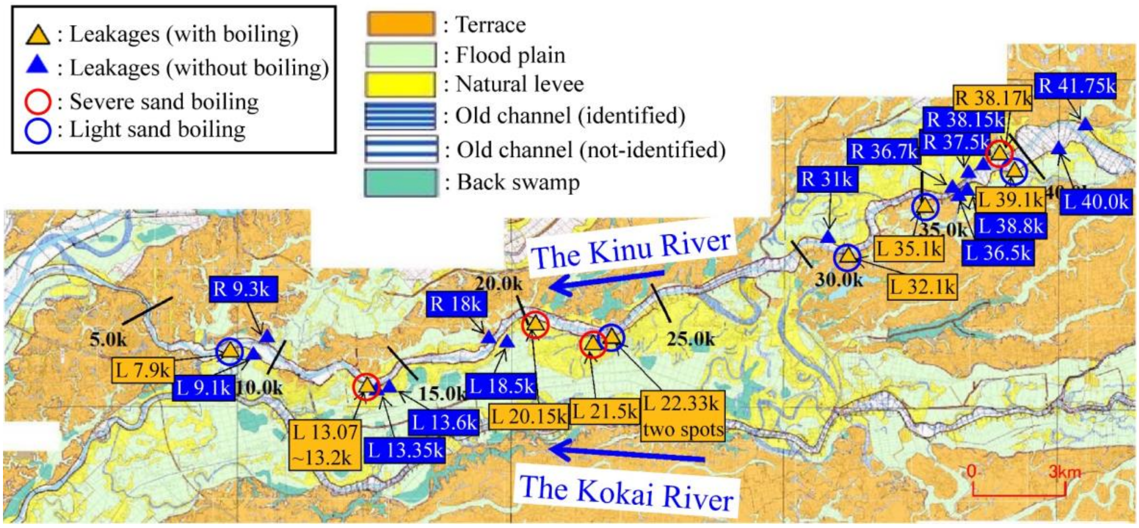

Figure 2. Distribution of the leakage events along the Kinu River after the "Kanto-Tohoku Heavy Rainfall" in 2015 (after KRDB MLIT, 2016).

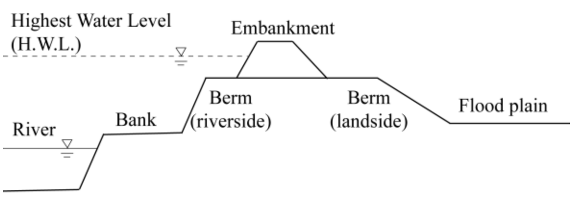

Figure 3. Conceptual model in the study.

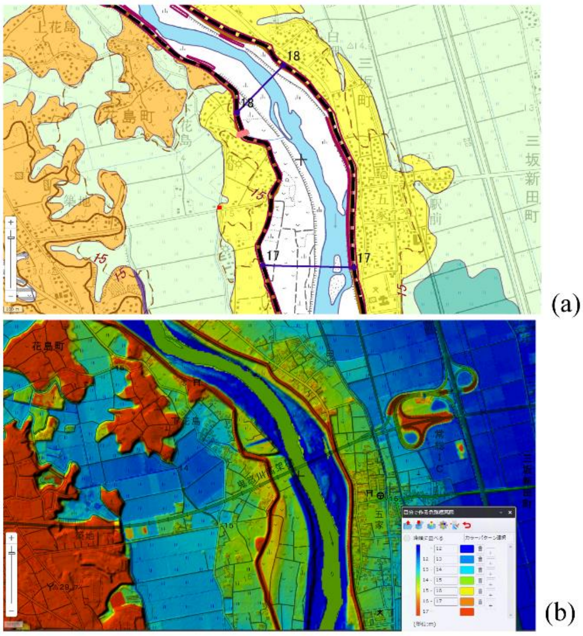

Figure 4. Different maps provided by the online GIS: (a) Landform Classification Map for Flood Control, (b) Elevation Map with self-defined coloured scale.

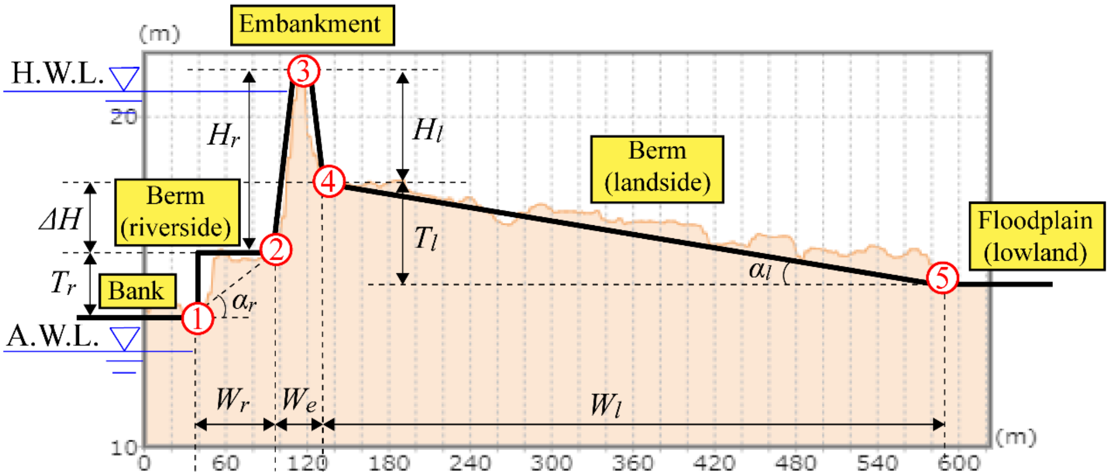

Figure 5. Schematic illustration of the proposed “embankment & berm” model.

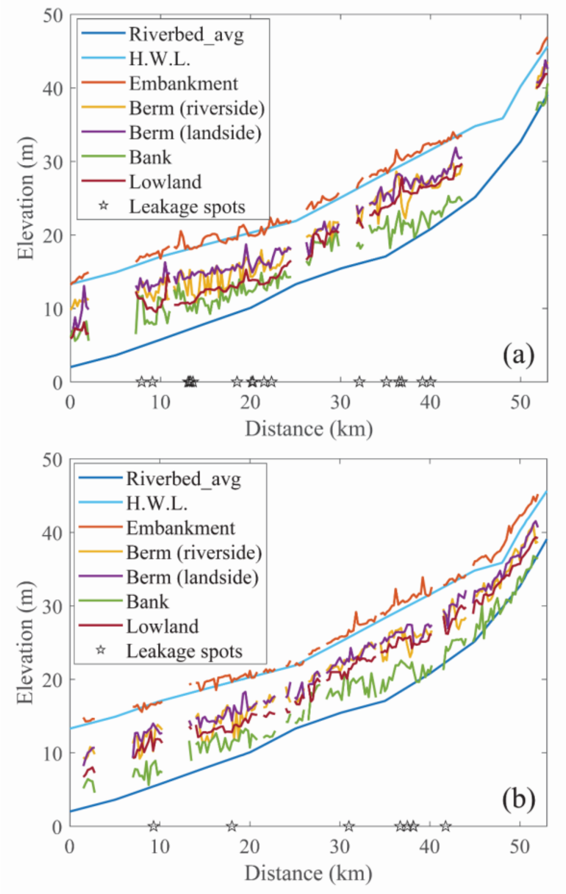

Figure 6. Elevation profiles along the river: (a) left bank, (b) right bank.

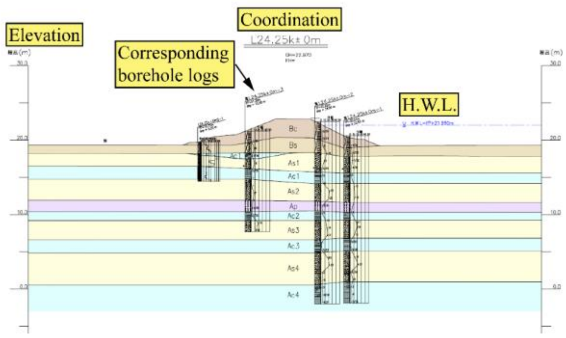

Figure 7. Typical soil profile in the database.

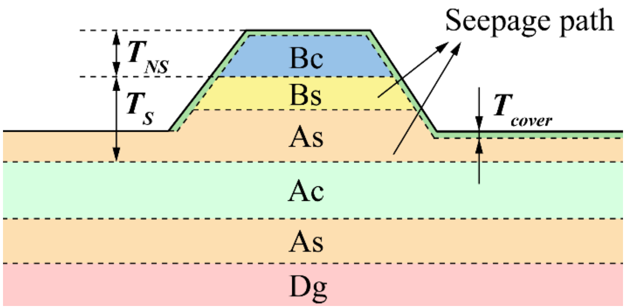

Figure 8. Definition of the “seepage path”.

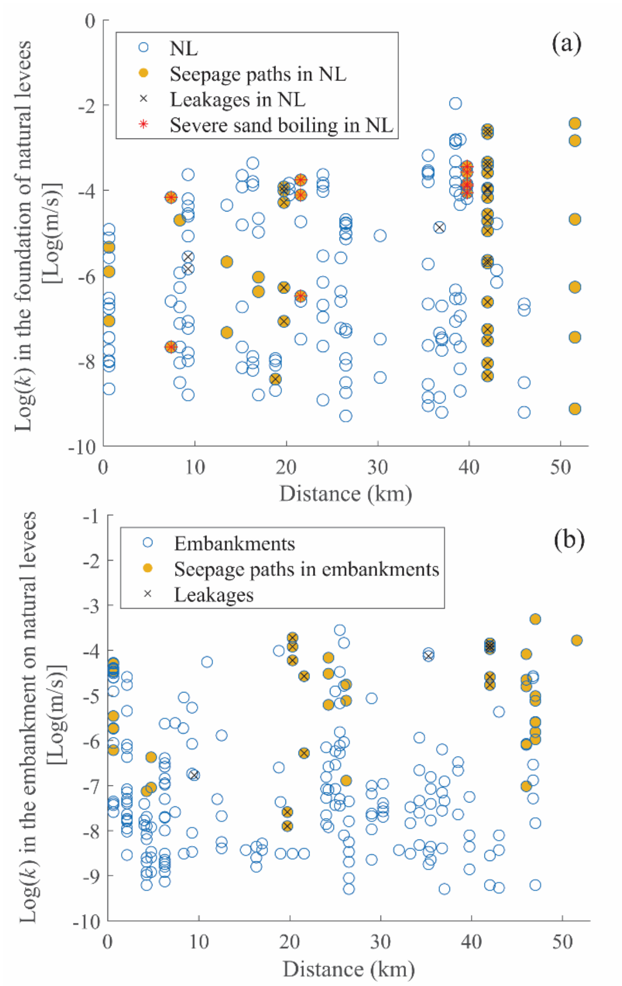

Figure 9. Spatial distributions of hydraulic conductivity (a) in the foundations of natural levees, and (b) in the embankments sitting on natural levees.

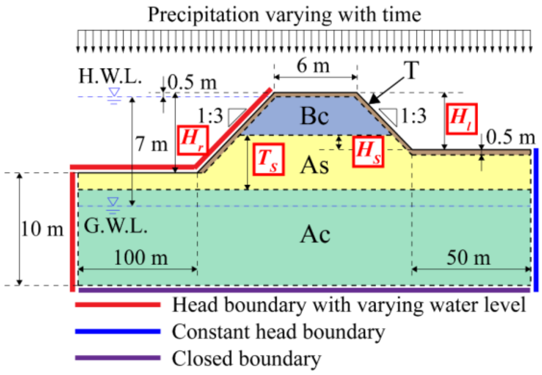

Figure 10. Schematic sketch of the simulated model (not in scale).

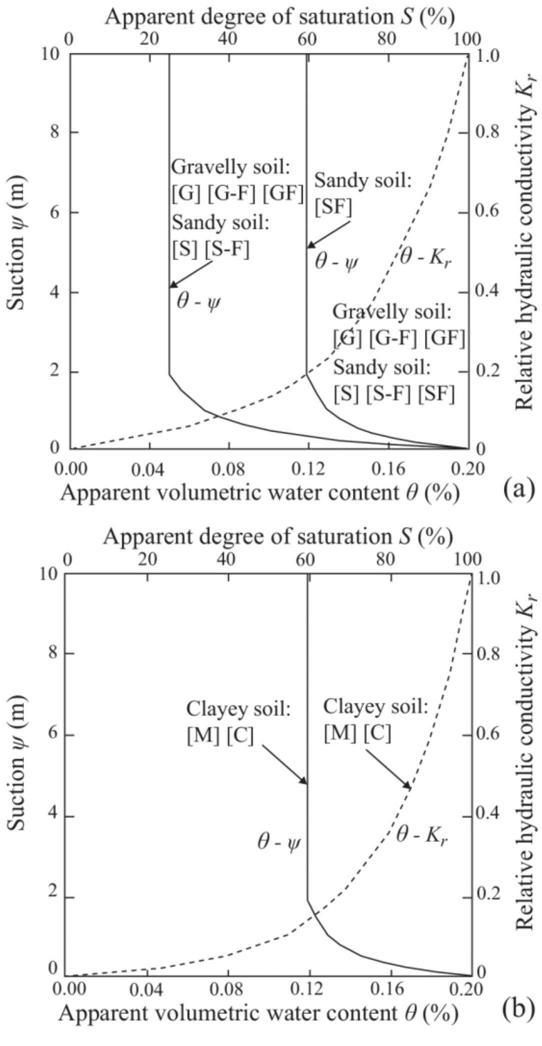

Figure 11. Unsaturated soil property for (a) gravelly and sandy soil, and (b) clayey soil (after JICE, 2012).

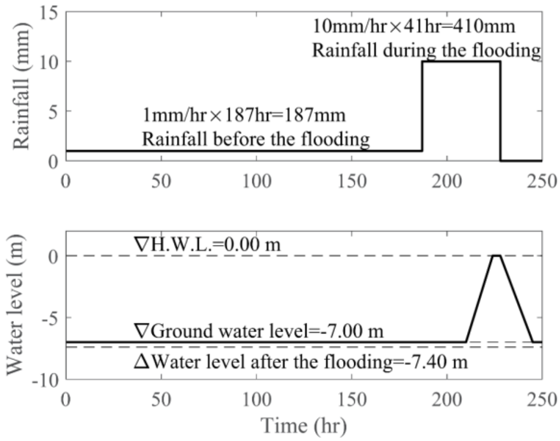

Figure 12. Input hydraulic loading of the simulated model.

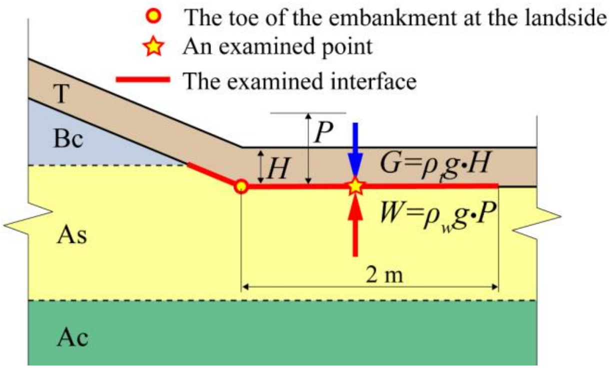

Figure 13. Illustration for the calculation of the index for piping G/W.

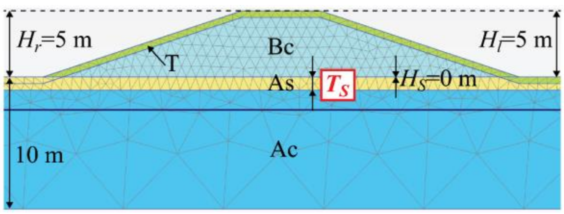

Figure 14. Simulated models in the study on the effects of the thickness of the seepage path (The snapshot is retrieved from Case 1-1).

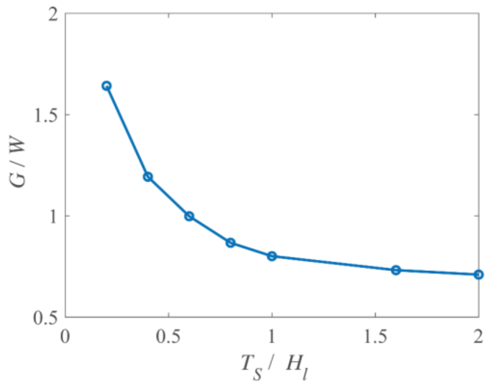

Figure 15. Index for piping risk G/W varying with the thickness of the seepage path T_S.

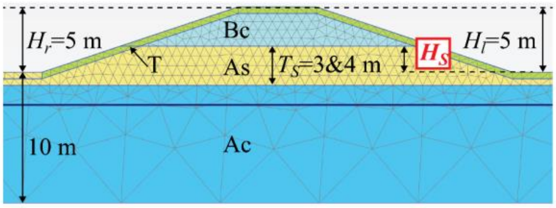

Figure 16. Simulated models in the study on the effects of the position of the seepage path (The snapshot is retrieved from Case 2-4).

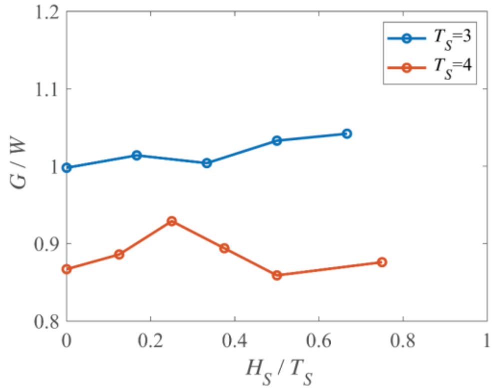

Figure 17. Index for piping risk G/W varying with the heights of the seepage path above the ground H_S.

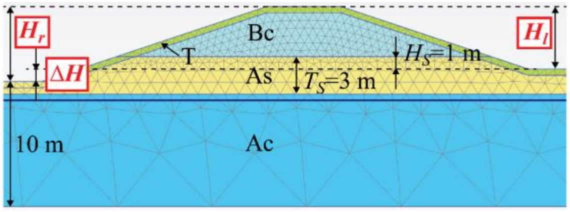

Figure 18. Simulated models in the study on the effects of the elevation difference between the landside and the riverside (The snapshot is retrieved from Case 3-6).

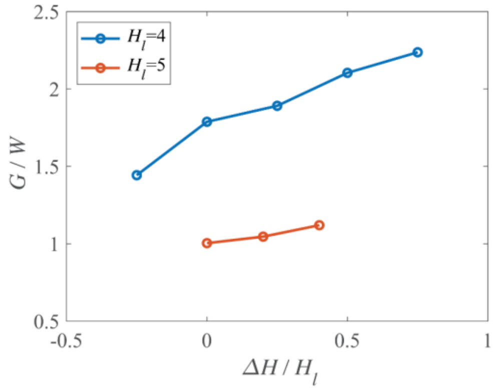

Figure 19. Index for piping risk G/W varying with the relative elevation of the toe of the embankment at the landside to that at the riverside ΔH.

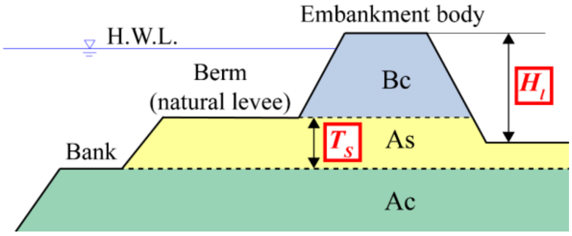

Figure 20. Typical geometry susceptible to leakages.

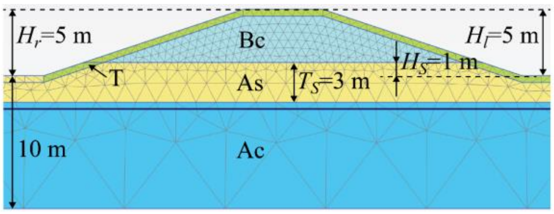

Figure 21. Simulated models in the study on the effects of the seepage paths (The snapshot is retrieved from Case 3-2).

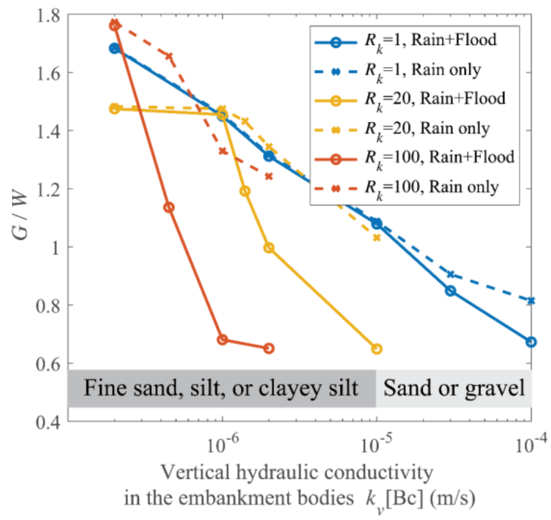

Figure 22. Index for piping risk G/W varying with the vertical hydraulic conductivity in the embankment bodies k_v[Bc].

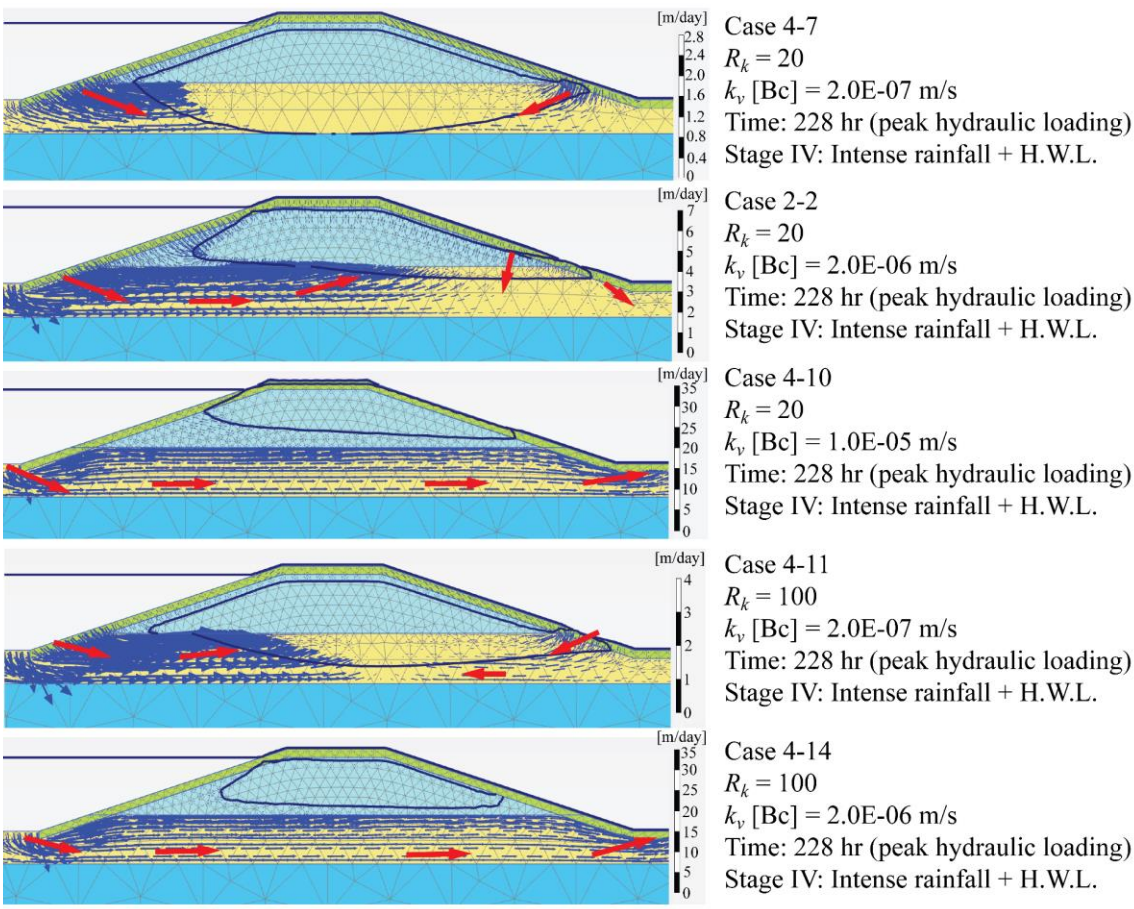

Figure 23. Comparison between the distributions of flow velocity under the peak hydraulic loading.

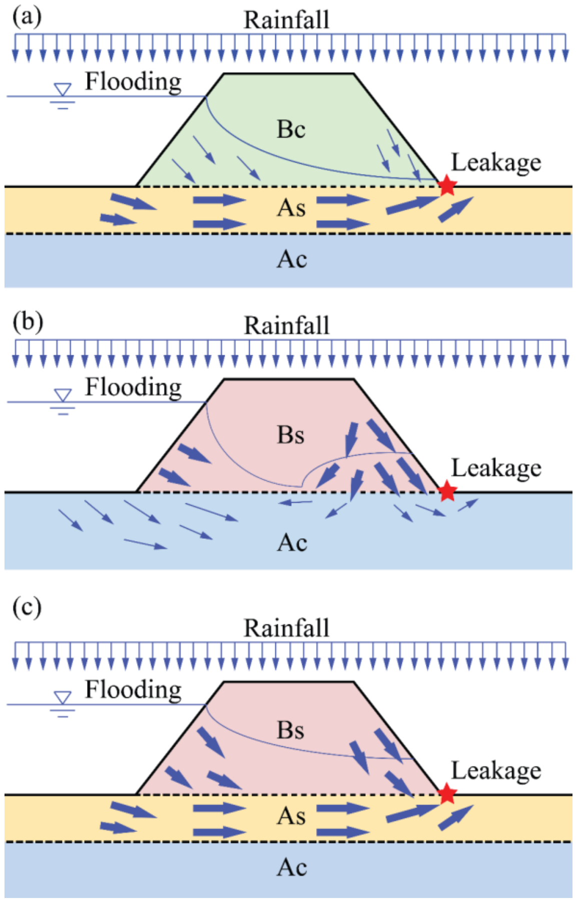

Figure 24. Schematic illustration of the leakage driven by (a) the seepage flow due to the flooding, (b) the surface infiltration due to the rainfall, and (c) the combined effect of the flooding and the rainfall.

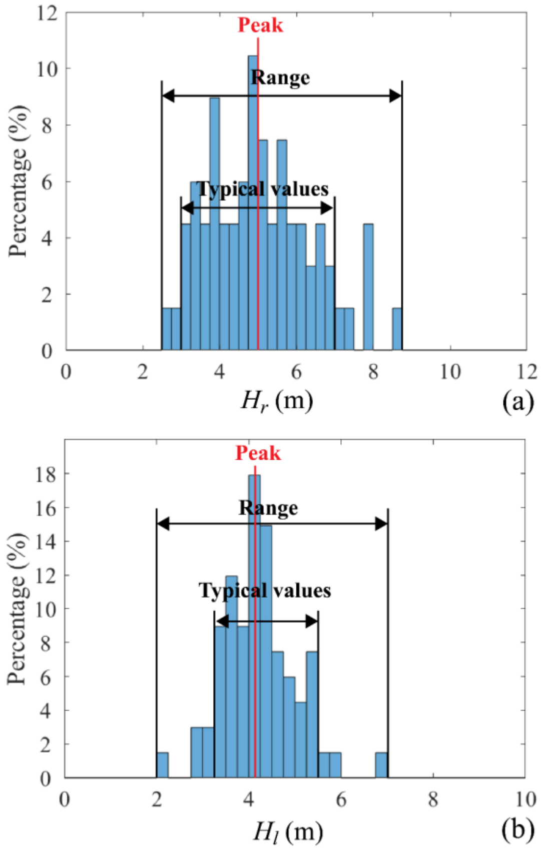

Fig. 25 Distributions of the (a) relative elevation of the embankment at the riverside H_r and (b) the relative elevation of the embankment at the landside H_l in the representative section.

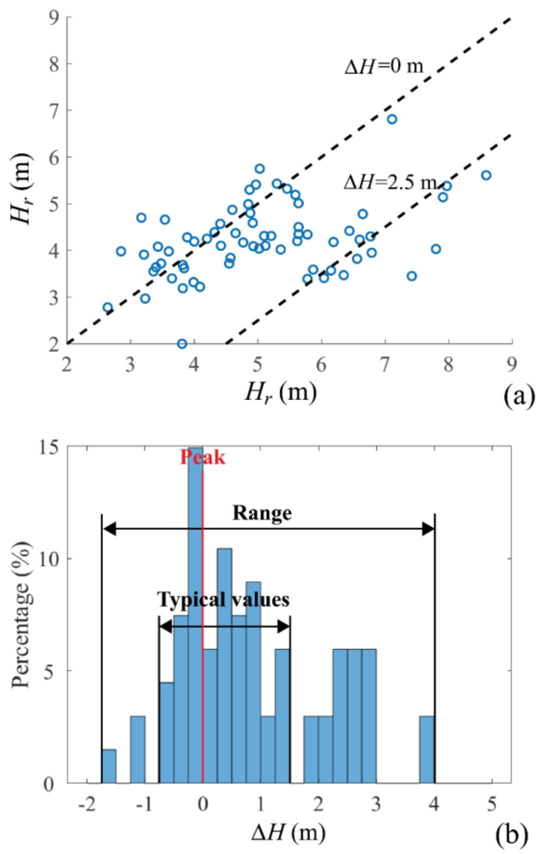

Fig. 26 (a) Combination of the relative elevation of the embankment at the riverside H_r and that at landside H_l in the representative section; (b) Distribution of the relative elevation of the toe of the embankment at the landside to that at the riverside ΔH in the representative section.

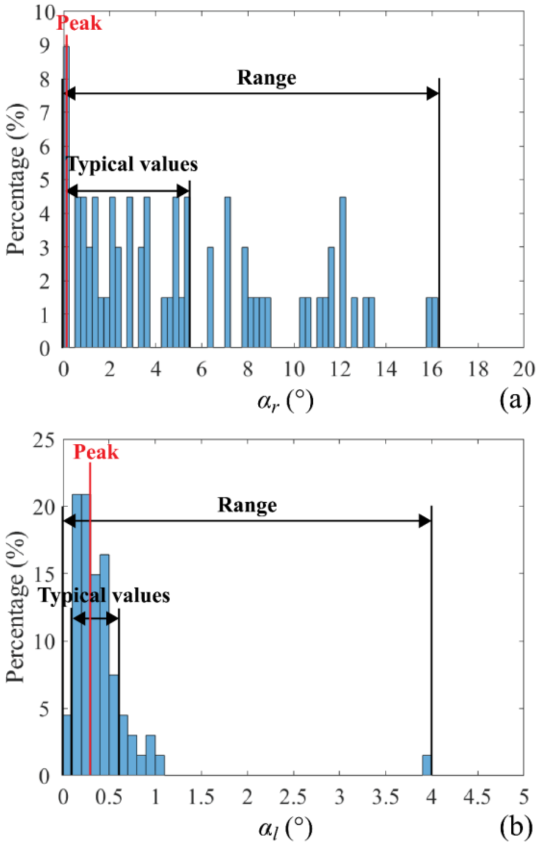

Fig. 27 Distributions of the slope of the berm α at the (a) riverside and (b) the landside in the representative section.

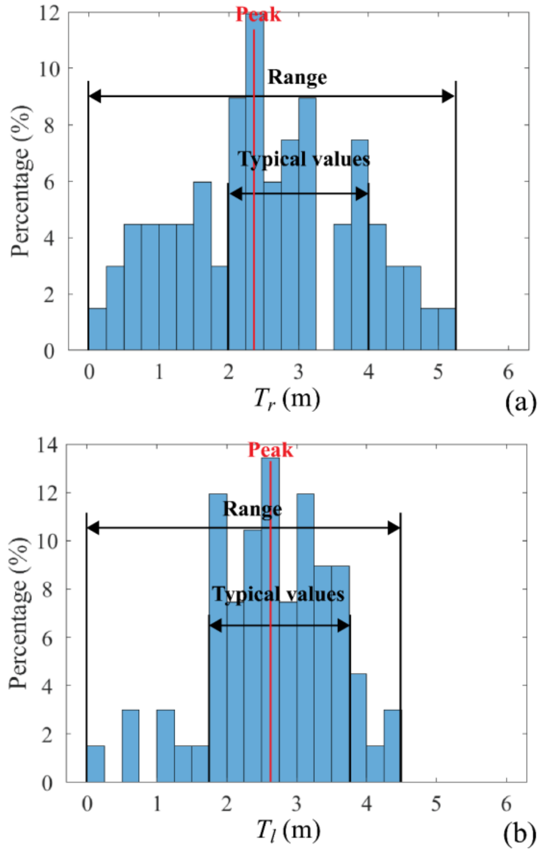

Fig. 28 Distributions of the berm thickness T at the (a) riverside and (b) the landside in the representative section.

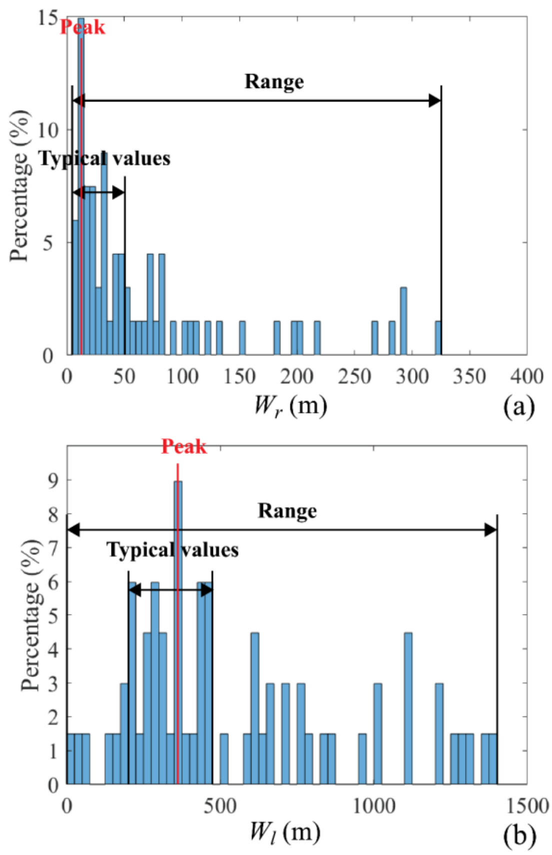

Fig. 29 Distributions of the berm width W at the (a) riverside and (b) the landside in the representative section.

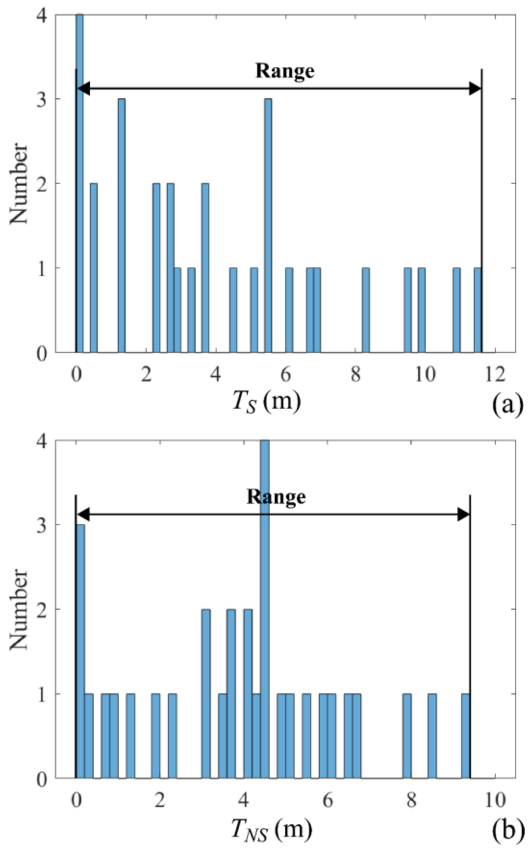

Fig. 30 Distribution of the (a) thickness of the seepage paths T_S and (b) thickness of the non-seepage paths in the representative section.

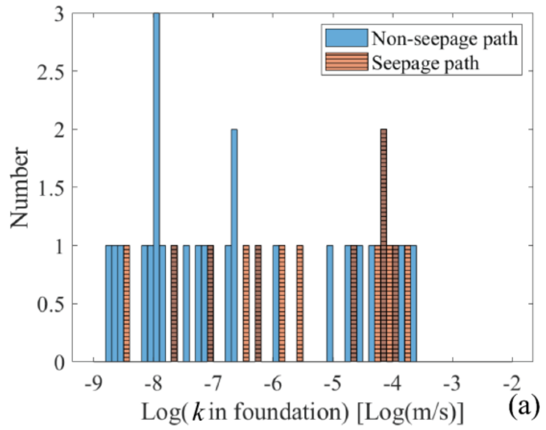

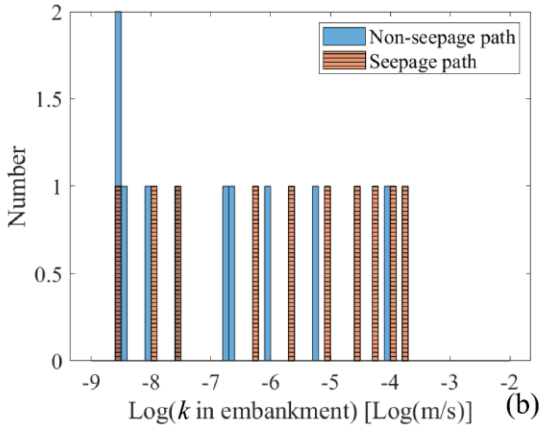

Fig. 31 Distribution of the hydraulic conductivity k estimated by Creager's method (a) in the foundations and (b) in the embankments in the representative section.